RESEARCH ARTICLE

Further steps towards the tuning of inertial controllers for broadband-frequency-varying structures

J. M. Soria[1]* | **I. M. Díaz**[1] | **J. H. García-Palacios**[2]

[1]Department of Continuum Mechanics and Theory of Structures, ETS de Ingenieros de Caminos, Canales y Puertos, Universidad Politécnica de Madrid, 28040 – Madrid, Spain.

[2]Department of Hydraulics, Energy and Environmental engineering, ETS de Ingenieros de Caminos, Canales y Puertos, Universidad Politécnica de Madrid, 28040 – Madrid, Spain.

Correspondence
J.M. Soria, Assistant Professor, Department of Continuum Mechanics and Theory of Structures, ETS de Ingenieros de Caminos, Canales y Puertos, Universidad Politécnica de Madrid, 28040 – Madrid, Spain.
Email: jm.soria@upm.com

Funding information
Ministry of Science, Innovation and Universities (Government of Spain), Research Project SEED-SD (RTI2018-099639-B-I00).

There is a large number of slender structures which are prone to vibrate due to pedestrian loads. The well-known Tuned Mass Damper (TMD) is increasingly used in practice, but this device may detune under several circumstances drastically reducing its expected performance. A Semi-active TMD (STMD) provides more robustness under structure uncertainties than the passive one and may be recommended for use when several vibration modes are in the excitation range and/or when the mode to cancel has uncertainty or varies over time. The tuning of the semi-active device for these cases cannot be the same as the passive one. This paper presents a methodology for the tuning of an STMD under broad frequency-band uncertainties using an ON/OFF phase control law. This control law is experimentally implemented considering interesting practical aspects, such as the estimation of the inertial mass velocity from the measured acceleration, or a low-pass filter to avoid unnecessary control actions, among others. An optimization process using a proposed performance index is carried out. Thus, it has been demonstrated that the optimal STMD is achieved for much lower damping and higher tuned frequency than the passive one. Finally, the proposed methodology is validated with experimental results.

KEYWORDS

semi-active control, vibration control, smart TMD, experimental results.

1 | INTRODUCTION

Lightweight and high-span pedestrian structures are usually prone to vibrate. Although current codes may be fulfilled, these structures may vibrate excessively and are not as comfortable as expected. Control devices can mitigate vibration significantly and improve comfort while fulfilling vibration serviceability requirements, simultaneously increasing the lifespan of the structures.

Vibration damping systems for civil structures are continuously being proposed. They can be classified into passive, active, semi-active and hybrid control. The Tuned Mass Damper (TMD) [1], referred also to as tuned vibration absorber, is the most commonly passive device used in footbridges [2]. A review of control devices implementation in landmark footbridges have been presented in [3, 4]. The main drawback of TMDs are that they are highly effective only over a narrow frequency band. Hence, when structures show modal properties changing over time, and/or several vibration modes [5, 6] must be cancelled by the same device, TMDs may detune and experience a significant loss of efficacy. Under these circumstances, the use of semi-active devices may become a competitive alternative [7, 8, 9]. However, several issues have to be tackled to achieve a successful implementation for broad frequency-band vibration: i) the design of the control law to implement, ii) the frequency tuning in passive mode, iii) the damping in passive mode, iv) the definition of a Performance Index (PI) able to represent the performance in a broad frequency band and v) practical issues such as filtering and switching on/off function. Some of these issues have been partially addressed previously [10, 11, 12].

Passive vibration control using TMDs [13, 14, 15] and optimal tuning have been extensively studied [16, 17]. The option to include more than one TMD has also been considered in order to increase its robustness and expand its frequency bandwidth [18]. In this sense, the Semi-active TMD (STMD) may be a solution that leads to better results in terms of costs and performance. The dynamic performance of this non-linear system has been studied in [10]. The application of this control technology may be used to solve a vibration problem [19, 20] or as an improvement of the structural design [21]. Numerous studies have been conducted emphasizing its performance robustness through tracking the force of the controllable damper device [22, 11]. Ferreira [12] studied an optimal tuning of the controller through a profound parametric study of the parameters of the STMD. Hence, neither they set a minimization problem based on a PI related to the vibration serviceability nor include the non-linear damper behaviour.

In the set of semi-active devices, magneto-rheological (MR) dampers are usually used as smart dampers [23]. The MR damper is a damper filled with an MR fluid capable of producing adaptive damping forces that are controlled by modifying the magnetic field applied in real time. In this case, the MR damper is used as the smart device in the control strategy, giving the following advantages: rapid response, large damping force with wide dynamic range and durability. Thus, an MR damper can be used within control systems. However, MR dampers have a strongly non-linear nature that has to be modelled and included in control design. Otherwise, the simulated performance may differ considerably from the experimental performance.

The control law used in this article was originally presented by Soong [24] and studied by other authors [25, 26, 27, 12]. The adapted version of [27] is a simple and focus-on-implementability semi-active control law that, according to the simulations carried out in [9, 28], produces promising results assuming an ideal viscous damper. Although sensitivity studies of its parameters have been accomplished, as well as optimal tuning proposals [12, 29], the main purpose of the semi-active device has not considered for its tuning: be effective in a broad frequency-band spectrum.

Cases such as modal properties varying with time due to external factors (temperature, level of occupancy or ageing) and structures with several vibration modes with closely-spaced frequencies prone to vibrate are common in practice [6]. Under these circumstances, much greater robustness than that provided by the TMD is required and a design approach that considers both uncertainties in structure modal parameters and an MR damper is desirable. Thus, the tuning of the semi-active system should take into account its broad spectrum of operation and the significant non-linearities, such as the control law itself, as well as the operation of the MR damper. Then, a new approach to tuning STMDs is carried out in this article and compared to the passive performance. Necessary aspects to implement the control law are also described and taken into account within the optimization problem. Although the problem is stated in a general way, this is clearly geared to highly resonant structures (for instance, lightweight footbridges) and the PI to be minimised is focused on user comfort. The following issues are considered: i) the velocity of the inertial mass should be estimated from its acceleration, ii) a continuous trigger function should be implemented in order to avoid unnecessary damper actions when structure acceleration is of low amplitude, and iii) acceleration of the structure should be carefully filtered to avoid spillover effects and unnecessary damper action when this signal is crossing over zero.

The paper continues with a description of the semi-active inertial controller and the vibration control strategy adopted in Section 2. A sensitivity analysis of the tuning parameters of the control device is carried out in Section 3. The effect of including damper force saturation and an MR damper model instead of a linear-viscous damper are also analysed. Lastly, an optimization procedure to tune the semi-active device is proposed. Section 4 shows the experimental results conducted on a steel beam and carefully explains the implementation of the semi-active control and the practical issues that have been considered. Finally, some conclusions and suggestions for future work are given in Section 5.

2 | SEMI-ACTIVE TUNED MASS DAMPER

2.1 | Tuned Mass Damper

A TMD consists of a secondary mass (also called moving or inertial mass) attached to the structure by means of springs and dampers. The TMD mass is fixed as a fraction of the modal mass of the unique targeted vibration mode; the stiffness of the springs is selected to obtain the optimum TMD frequency, and the viscous damper ensures the operation of the TMD in a range of frequencies around the tuning frequency (providing a certain robustness for a frequency bandwidth while degrading performance at the tuning frequency). However, they have a relatively poor performance for low-level vibrations and they still exhibit a significant lack of performance due to the off-tuning issue.

Figure 1a shows the model of a classical TMD composed of an inertial mass m_T attached to a primary system by means of a spring of constant k_T and a viscous damper of constant c_T. The primary system is the structure modelled as a single Degree Of Freedom (DOF) system, which is composed of a mass m_S, a spring of constant k_S and a viscous damper of constant c_S.

The TMD has been designed using the approximate solution provided by Asami and Nishihara [30], based on H_∞ optimization for primary systems with vanishing damping. The expressions by Asami and Nishihara [30] minimize the acceleration which is related with potential applications in footbridges and also to assess the pedestrian comfort. The

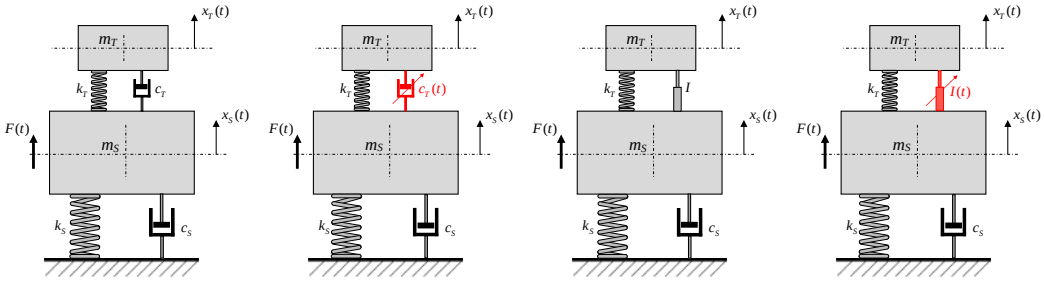

(a) TMD control. (b) STMD control. (c) MR-TMD control. (d) MR-STMD control.

FIGURE 1 Model of the 2-DOF systems studied. Red symbol (↗) means changing over time.

TMD properties when the primary system acceleration under harmonic excitation is minimized are:

$$\eta = \sqrt{\frac{1}{1+\mu}} \tag{1}$$

$$\zeta_T = \sqrt{\frac{3\mu}{8(1+\mu)^3}} \cdot \sqrt{1+\frac{27}{32}\mu}, \tag{2}$$

in which $\mu = m_T/m_S$ is the mass ratio, $\eta = \omega_T/\omega_S$ is the frequency ratio and the stiffness and damping coefficient for the TMD are obtained from:

$$k_T = \omega_T^2 m_T \tag{3}$$

$$c_T = 2\zeta_T m_T \omega_T, \tag{4}$$

respectively. This solution is the initial solution for the optimization process presented in Subsection 2.3.

2.2 | Semi-active control strategy

A phase control strategy for the TMD damping is considered here (see Figure 1b). The phase control presented in [24, 26] and adapted by [27] has been adopted since this is clearly geared to practical implementation due to the measured real-time parameters employed: the structure acceleration instead of displacement and the inertial mass velocity instead of the relative velocity. This control law will then be effective when structure velocity is negligible with respect to the inertial mass velocity, which usually happens in civil engineering structures under resonant events. The lowest structural response is achieved when the velocity of the inertial mass and structure acceleration have opposing phases, so the semi-active device objective is to bring the inertial mass motion as close as possible to this phase. This is equivalent to a phase lag of 90º between the structure acceleration and the control force. The control law adopted is of the ON/OFF type due to its simplicity. Thus, the adopted control law when ideal viscous damping is assumed is defined as:

$$\begin{cases} \ddot{x}_S \cdot \dot{x}_T \leq 0 & \Rightarrow \quad c_T = c_{\min} \quad \text{(normal functioning)} \\ \ddot{x}_S \cdot \dot{x}_T > 0 & \Rightarrow \quad c_T = c_{\max} \quad \text{(blocking functioning)}, \end{cases} \tag{5}$$

in which c_{max} is the maximum damping achieved by the damper, c_{min} is the optimal damping obtained from Eq. (4), $\ddot{x}_S$ is the structure acceleration (measured by an accelerometer) and $\dot{x}_T$ is the velocity of the inertial mass (which might be obtained from the integration of an accelerometer signal installed on the inertial mass). When an MR damper is assumed (see Figure 1d), the law of Eq. (5) is rewritten as follows:

$$\begin{cases} \ddot{x}_S \cdot \dot{x}_T \leq 0 & \Rightarrow \quad I = I_{min} \quad \text{(normal functioning)} \\ \ddot{x}_S \cdot \dot{x}_T > 0 & \Rightarrow \quad I = I_{max} \quad \text{(blocking action)}, \end{cases} \tag{6}$$

in which I is the current applied to the MR damper. The maximum and minimum value, I_{max} and I_{min}, depend on the MR damper employed. This strategy is fairly simple and implementable as it uses only two magnitudes easily measured. However, a few aspects must be taken into account before the practical implementation. These are described in Subsection 4.3.

2.3 | Optimal control design

The purpose of this section is to provide a procedure to find an optimal tuning for STMD control devices in structures with uncertainty in their modal parameters and/or with several critical vibration modes. The term closed-loop control implies the use of a feedback controller to bring the output of the system (movement of structure) to a desired value. The controller changes the dynamics of the system. The general feedback control scheme is shown in Figure 2, in which the inertial controller changes in real time following the semi-active control law.

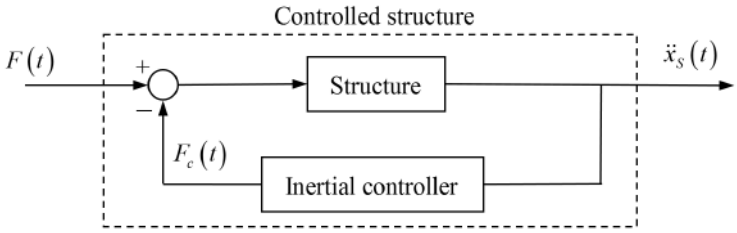

FIGURE 2 Simplified control scheme with an inertial controller.

The optimization will minimize a PI over a broad frequency band which is geared to structures that show resonant behaviour. The PI is defined according to the following expression:

$$\text{PI} = \max\left(\sum_{i=1}^{N} \hat{S}_i(\omega)\right) \quad \text{with} \quad \hat{S}_i = \frac{1}{F_0} S_i(\omega), \tag{7}$$

in which F_0 is the force amplitude of $F(t)$, $S_i(\omega)$ is the spectrum of the acceleration response of the structure $(\ddot{x}_S(t))$, $\hat{S}_i(\omega)$ is denoted as the normalized spectrum and N may be the number of vibration modes to be cancelled or a set of models representative of a particular uncertain vibration mode. This set may be derived considering a normal distribution of the modal parameters. Note that the $\hat{S}(\omega)$ is used instead of the frequency response function due to control system non linearities. The optimization problem consists of minimizing the PI defined in Eq. (7) subjected to

the following constraints:

$$\min_{f_T,\zeta_T} \text{(PI)} \quad \text{subject to} \begin{cases} f_T > 0 \\ \zeta_T > 0 \\ |x_T| \leq \text{maximum stroke} \end{cases}, \tag{8}$$

in which f_T and ζ_T are the frequency and damping ratio of the controller device. The variable $|x_T|$ is the displacement of the inertial mass that must be limited by the maximum stroke and μ is considered fixed. Note that in Eq. (8), the damping ratio ζ_T, equivalent to c_{min} in Eq. (5), is substituted by I_{min} (see Eq. (6)) when the MR damper model is included in the design.

The perturbation force $F(t)$ used to evaluate the structural response is a chirp waveform whose frequency increases at a linear range with time, as follows:

$$F(t) = F_0 \cdot \sin(2\pi f(t)\, t), \tag{9}$$

where the instantaneous excitation frequency is defined as a function of time (t):

$$\begin{aligned} f(t) &= f_i + kt, \\ k &= \frac{f_f - f_i}{T_f}, \end{aligned} \tag{10}$$

k being the rate of frequency change, f_f the final frequency, f_i the starting frequency and T_f the required time to sweep from f_i to f_f. The frequency range is chosen to excite a broad frequency band and T_f is chosen to ensure that sweeping at each frequency is sufficiently slow.

3 | SIMULATION RESULTS

Two kinds of analysis, described in Subsection 3.1 and 3.2, are carried out for the four configurations model shown in Figure 1. The first analysis is a sensitivity analysis of the tuning parameters of the control device. The second one consists of running the optimization procedure defined in Eq. 8.

3.1 | Sensitivity analysis

The following parameters have been adopted to undergo the sensitivity analysis:

- The excitation has been applied using a chirp signal (see Eq. 9) with an amplitude of 50 N, linear-varying frequency from 0.1 and 6 Hz and a sampling frequency of $f_r = 500$ Hz for a record of 500 s.
- The structure parameters are: $m_S = 500$ kg, $f_S = 2$ Hz and $\zeta_S = 0.05$.
- The inertial controller parameters are variables: $f_T \in (0.1 \cdot f_S,\ 2 \cdot f_S)$ Hz and $\zeta_T \in (0.01,\ 0.20)$ for TMD and STMD with viscous damping (Figures 1a and 1b, respectively), and $I \in (0,\ 0.5)$ A for MR-TMD and MR-STMD (Figures 1c and 1d, respectively).
- The mass ratio is constant, $\mu = 0.02$.

Table 1 shows the parameters used in the sensitivity analysis. The PI is studied for the tuning frequency ratio η and the damping ratio ζ_T. A total of 2601 simulations have been carried out. The inclusion of the MR damper model aims to study the effect of degradation in the operation of the control device, passive and semi-active.

TABLE 1 Parameters used for the sensitivity analysis.

Parameter	Value
Mass, m_S (kg)	500
Damping ratio, ζ_S (%)	0.5
Frequency, f_S (Hz)	2.0
Mass ratio, μ	0.02
Inertial mass, m_T (kg)	10
Maximum damper force saturation, $F_{D_{\max}}$ (N)	75
Chirp amplitude, F_0 (N)	50
Chirp initial frequency, f_i (Hz)	0.1
Chirp final frequency, f_f (Hz)	6.0

3.2 | Control design parameters

Having completed the sensitivity study, the optimization problem is run. The stroke of the device has been limited to 0.3 m and the value of the mass ratio has been set again at 2%. Note that both variables are related, the higher the mass ratio is, the smaller the stroke achieved.

The PI minimization has been computed using the `patternsearch` function from MATLAB software [31]. The pattern-search method seeks a minimum based on an adaptive mesh that, in the absence of linear constraints, is aligned with the coordinate directions [32]. Several optimization algorithms have been compared and pattern-search has always been the most efficient in achieving the best solution.

The optimization is carried out assuming that the parameters involved are variables following a normal distribution randomly generated. Each varying parameter has the following characteristics: $f_S \sim \mathcal{N}(2,\, 0.2)$ Hz, $\zeta_S \sim \mathcal{N}(1,\, 0.5)$ %, $m_S \sim \mathcal{N}(500,\, 100)$ kg and $F_0 \sim \mathcal{N}(50,\, 25)$ N, in which $\mathcal{N}(\mu_i,\, \sigma_i^2)$ indicates the normal or Gaussian distribution with μ_i and σ_i^2 being the mean and the standard deviation, respectively. Each randomly generated value of each parameter is grouped with those that occupy the same position in the generation sequence, obtaining a set of randomly generated models for the same structure. The PI has been computed from 100 models, that is, $N = 100$ in Eq. (7).

3.3 | Ideal viscous damper

The sensitivity analysis presented in 3.1 is carried out for TMD and STMD. For the latter, only the $c_{\min}$ is tuned since $c_{\max}$ is assumed to be enough for blocking (see Eq. (5)). The PI is computed for each case. Figure 3 shows the contour plots including isolines. It is clear that the STMD is more robust than the TMD.

How the PI is obtained is explained here. Firstly, the set of randomly-generated models is obtained (Figure 4a). Then, Figure 4b shows the result of Eq. 8, in which the maximum value of the sum of the spectra is the PI.

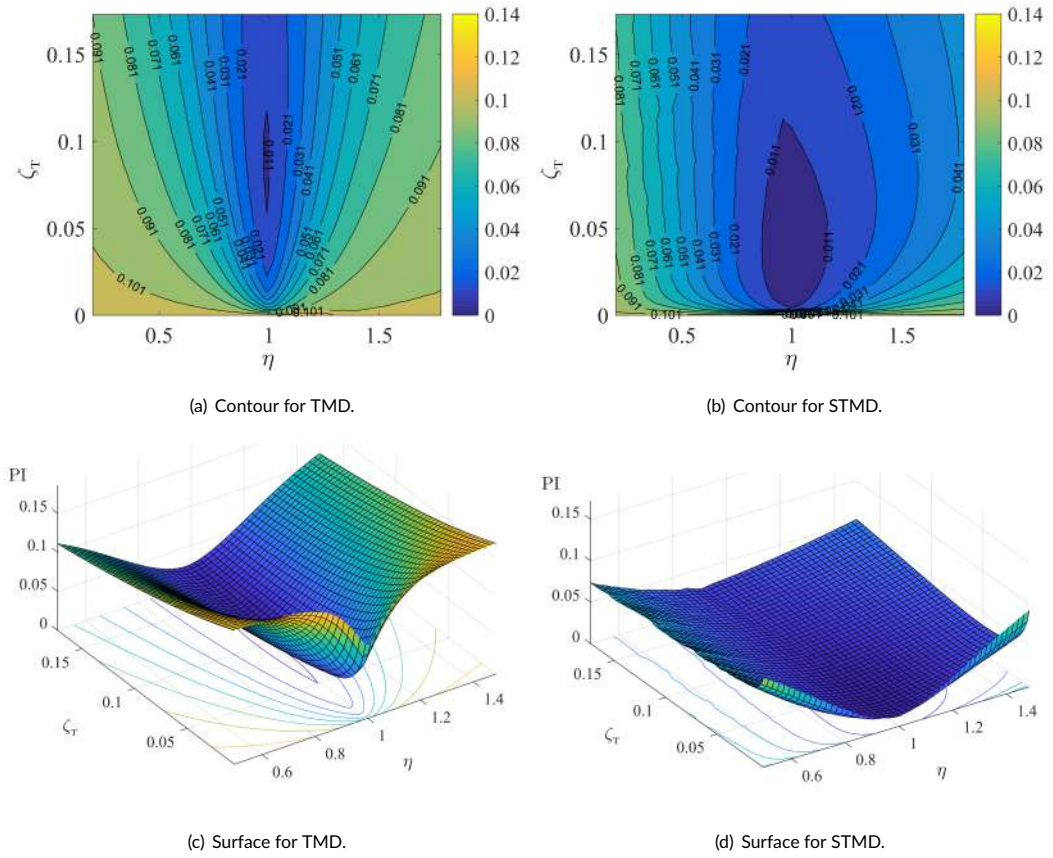

(a) Contour for TMD.

(b) Contour for STMD.

(c) Surface for TMD.

(d) Surface for STMD.

FIGURE 3 Contour plot of the PI for TMD and STMD with linear-viscous damper.

Figure 5 shows the envelope curve of the PI with the initial solution together with the optimized one obtained for passive (Figure 5a) and semi-active (Figure 5b). Although the maximum value of the curve (PI) is the value to be optimized, it must be appreciated that all the points of the curve in the semi-active case are below that of the passive case. Table 2 shows a summary of the results associated to Figures 5a and 5b. On the one hand, the optimum design of the TMD improves the PI obtained from the classical approach (Eq. (1) and Eq. (2)). To achieve this, the TMD damping should be much greater in order to deal with the system uncertainty. On the other hand, for the considered control law, the optimal design parameters achieved significantly improves the performance reduction, and interestingly, the unblocking damping of the STMD should be much slower than the one obtained from the classical approach.

3.4 | Effect of damper force saturation

Now, a maximum damper force is added to the model: the force saturation. All the cases shown in Figure 3 are repeated with different force saturation values in order to evaluate the performance degradation of the device since

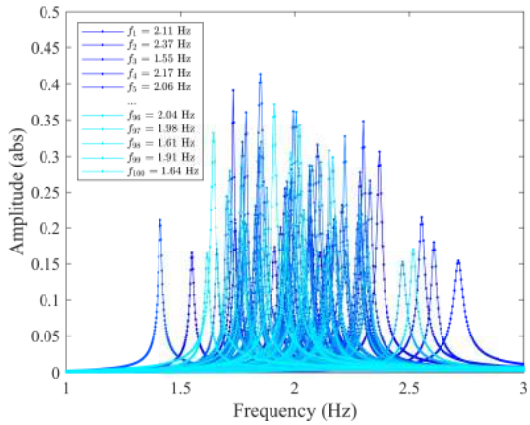

(a) $\hat{S}_i$ of each case of modal parameters uncertainties.

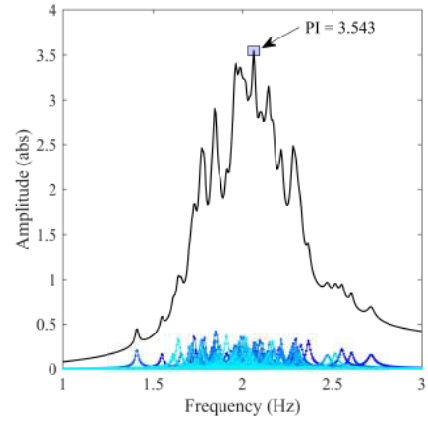

(b) $\sum \hat{S}_i$, envelope curve obtained from Figure 4a. The maximum value is the PI.

FIGURE 4 Uncontrolled case. Obtaining the PI.

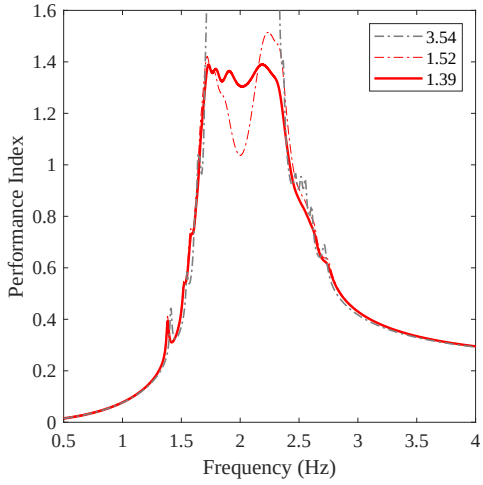

(a) TMD.

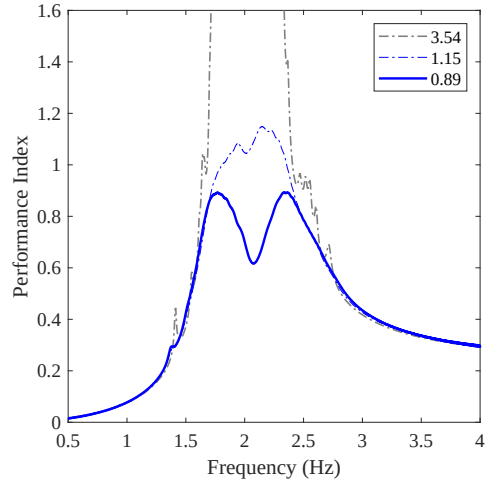

(b) STMD.

FIGURE 5 Envelope curve and PI. Optimization for the case of viscous damping. The legend shows the PI values for these cases: (– – –) uncontrolled, (– – – – –) initial solution and (——) optimized solution.

its capacity to block is limited, that is:

$$F_D = c_{\max}\left(\dot{x}_T - \dot{x}_S\right) \leq F_{D_{\max}}. \tag{11}$$

TABLE 2 Results from the optimization procedure for TMD and STMD. The improvement is computed from the initial solution of each device.

Control device	f_T (Hz)	ζ_T (%)	PI	Reduction (%)	Improvement (%)
Uncontrolled structure	–	–	3.54	–	–
TMD (Asami)	1.98	8.65	1.52	57.06	–
TMD (Optimal)	2.02	13.25	1.39	60.73	↑ 3.67
STMD (Asami)	1.98	8.65	1.15	67.51	–
STMD (Optimal)	2.08	3.80	0.89	74.86	↑ 7.35

The running root mean square (RMS) acceleration computed using a τ-second time interval is defined as:

$$a_{\mathrm{RMS},\tau}(t) = \sqrt{\frac{1}{\tau}\int_{t-\tau}^{t} a^2(\tau)\, dt}. \tag{12}$$

The maximum value of the running RMS acceleration with $\tau = 1$s is usually known as the Maximum Transient Vibration Value (MTVV):

$$\mathrm{MTVV} = \max\left(a_{\mathrm{RMS},1}(t)\right). \tag{13}$$

This value is used to asses the vibration serviceability of structures under human loading [33]. The Cumulative Distribution Function (CDF) curves for the MTVV are plotted in Figure 6a for several values of $F_{D_{\max}}$ (without control and with the TMD are also included for comparison). For the case of the TMD, $F_{D_{\max}}$ has no effects since demanded forces are always lower than that value. For the STMD, increasing the values of $F_{D_{\max}}$ improves the performance, since the blocking capacity is enhanced. In order to have a single value to compare the results with different $F_{D_{\max}}$, the total area between the CDF curve and the y-axis is obtained, resulting in Figure 6b. Thus, this figure shows the performance of each case referred to the case of 500 N (which is considered as perfect blocking). Initially, small $F_{D_{\max}}$ increments produce important performance improvements; however, from a certain $F_{D_{\max}}$ value, the increments do not result in significant performance improvements. With only $F_{D_{\max}} = 75$ N, 95% of the maximum performance is achieved.

3.5 | Effect of considering an MR damper model

In order to consider the MR damper model in the controller design, a model identification of the MR damper used for the experimental test was carried out. A Bingham model was identified. The objective is to study how the TMD and STMD performances degrade when an MR damper model is considered (MR-TMD, Figure 1c and MR-STMD Figure 1d) instead of an ideal viscous damper. This model assumes that a body behaves as a solid until minimum yield stress is exceeded and that it exhibits a linear relationship between the stress and the rate of shear deformation [34]. From the equilibrium of the mechanical element configuration, the force generated by the MR damper can be expressed as:

$$F_D(t) = c_0\,\dot{x} + f_c\,\mathrm{sign}(\dot{x}) + f_0, \tag{14}$$

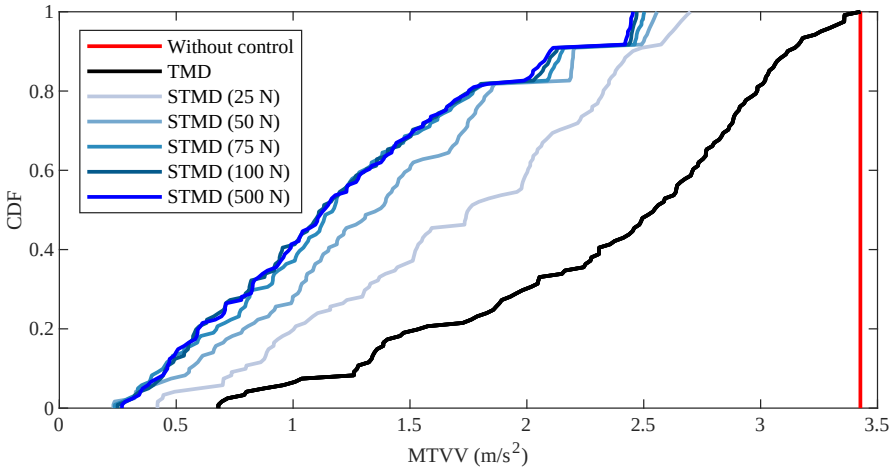

(a) CDF curves of the MTVV for several $F_{D_{\max}}$.

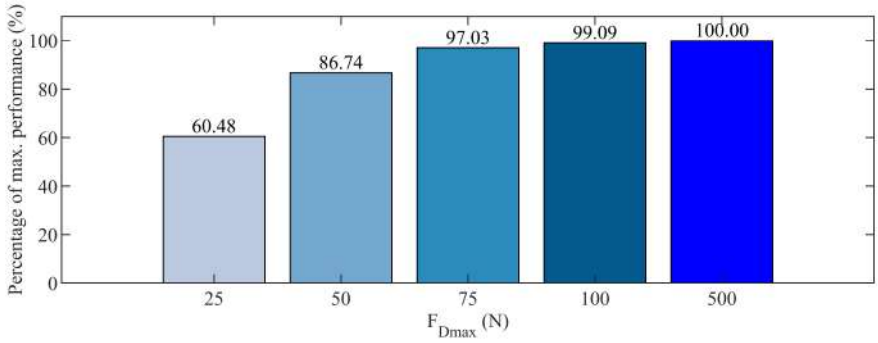

(b) Percentage of the maximum performance for several $F_{D_{\max}}$.

FIGURE 6 Performance in terms of the CDF of the MTVV for several damper force saturations $F_{D\max}$.

where c_0 is the viscous damping parameter, f_c is the frictional force and f_0 is the force offset. Several experimental tests were carried out for several combinations of displacements, frequencies and damper currents in order to calibrate the damper response of the numerical model. Figure 7 shows the experimental setup together with the MR damper to be identified: sponge-type magneto-rheological damper from the Lord Corporation company. A steel frame combined with an electromagnetic actuator (APS Dynamics Model 400), an accelerometer, an LVDT and a load cell have been used in order to measure the damper acceleration, the displacement, and the force, respectively. Each test was done with a sinusoidal excitation with fixed frequency, fixed shaker gain (amplitude displacement measure by an LVDT) and fixed damper current. This process has been repeated for several combinations. Therein, the damping ratio is changed by the input current of the MR damper. The selected range of frequencies, shaker gains and current supplies involved in the experimental procedure are specified in Table 3. A total of 252 tests were completed.

Figure 8a shows, in a single plot, all the parameters involved in the identification process. The amplitude of the force, displacement and acceleration in the steady-state response of each test are shown. Figure 8b shows that

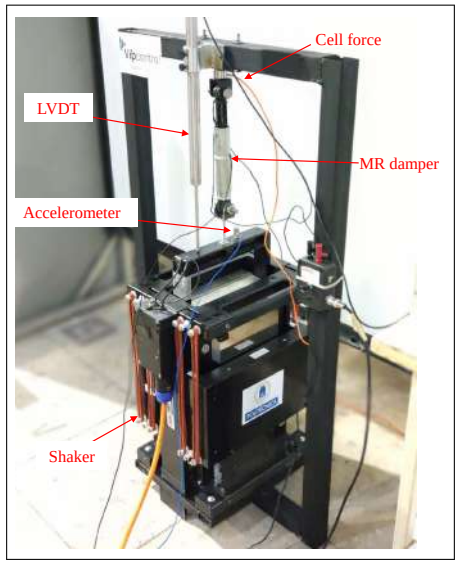

FIGURE 7 Experimental setup for MR damper model identification.

TABLE 3 Variation range of the input parameters for the MR damper identification.

Parameter	Range
Shaker gain (V)	0.05 to 0.8
Frequency (Hz)	1 to 7
Input current I (A)	0 to 0.5

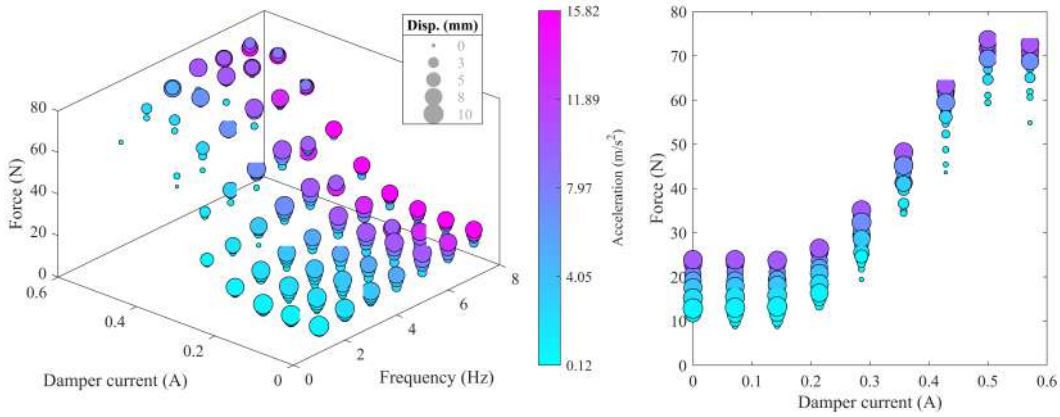

FIGURE 8 Summary of the experimental results conducted for the identification of the MR damper model.

the dependency of the acceleration with the displacement and the frequency is much lower than that with the input current, in such a way that the Bingham model parameters are considered to be dependent only on the current I. Thus, the parameters of the model of Eq. (14) were calibrated using `lsqcurvefit` MATLAB routine (least-square method) and these are:

$$\begin{aligned} f_c &= -0.40I^3 - 0.67I^2 + 0.92I + 0.02 \quad [\text{N}] \\ c_0 &= -28.40I^3 + 25.22I^2 + 8.32I + 0.05 \quad [\text{N s/mm}] \\ f_0 &= 0 \quad [\text{N}]. \end{aligned} \tag{15}$$

Hence, the control law adopted is the one of Eq. (6) and the initial condition for the optimization process will be assumed for $I = 0$ A. For the semi-active case, it is necessary to optimize the minimum damper current, because the current to block the inertial mass is the maximum value for the ON/OFF control law. Figure 9 shows the degradation obtained when the Bingham MR damper model is used for the sensitivity analysis with the MR-TMD and the MR-STMD. The following aspects are observed from Figure 9 as compared to Figure 3: i) in both cases, the performance has degraded clearly when the MR model is considered and ii) the MR-STMD behaves much better than the MR-TMD, showing a greater robustness, i.e., it is more effective for a broader frequency band.

The optimization analysis for designing the control parameters is carried out for MR-TMD and MR-STMD. Figure 10 shows the PI obtained for both cases. The PI of the MR-TMD is almost the same as that of the TMD (see Figure 5a). However, the PI of MR-STMD is worse than the STMD (see Figure 5b), so the inclusion of the MR model significantly degrades the effectiveness of the semi-active control. Table 4 shows the initial tuning and that obtained from the optimization process. Interestingly, the tuning frequency for the MR-STMD is over the structure frequency when a broad frequency band is considered. Besides, the optimal minimum current is $I_{\text{min}} = 0$ A, which indicates that the frictional force f_c of the device is excessive at 0 A and the results would improve significantly for lesser values of f_c.

TABLE 4 Results from the optimization procedure for the MR-TMD and the MR-STMD. The improvement is computed from the initial solution of each device.

Control device	f_T (Hz)	I (A)	PI	Reduction (%)	Improvement (%)
Uncontrolled structure	–	–	3.54	–	–
MR-TMD (Asami)	1.98	0.00	1.54	56.50	–
MR-TMD (Optimal)	2.02	0.05	1.40	60.45	↑ 3.95
MR-STMD (Asami)	1.98	0.00	1.18	66.67	–
MR-STMD (Optimal)	2.08	0.00	1.10	68.93	↑ 2.26

4 | EXPERIMENTAL RESULTS

4.1 | Structure description and experimental setup

The structure is a simply-supported steel beam of 5.10-meter span with UPN-200 cross-section. The structure is excited at mid-span, where the first vibration mode has its maximum sag, by the same actuator used for the MR

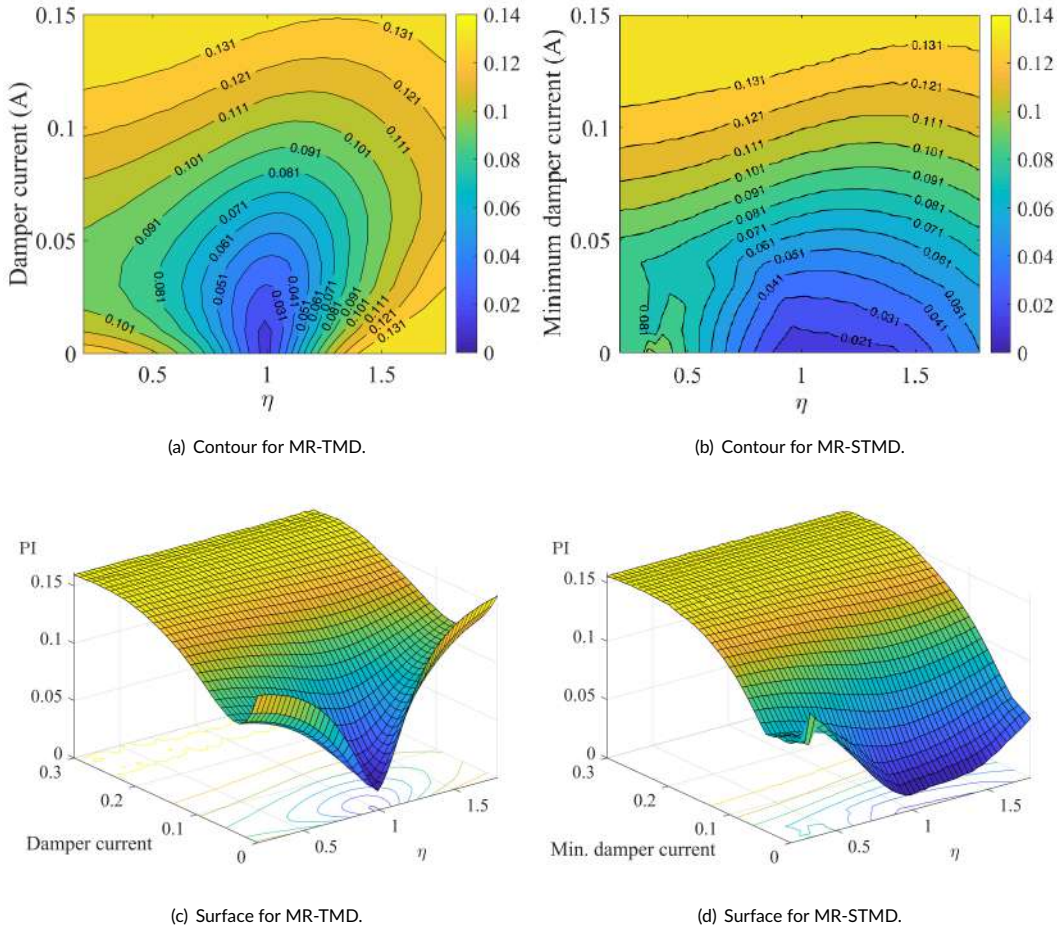

(a) Contour for MR-TMD.

(b) Contour for MR-STMD.

(c) Surface for MR-TMD.

(d) Surface for MR-STMD.

FIGURE 9 Contour plot of the PI for MR-TMD and MR-STMD with the Bingham MR damper model.

damper identification setup (see Figure 7). Two piezoelectric accelerometers mounted on a magnet-plate are attached to the beam and the inertial mass, respectively. The controller hardware is a CompactRIO from National Instruments using the LabVIEW real-time module. To carry out the control law (see Eq. (6)), the inertial mass velocity has to be estimated from its acceleration. Therefore, the control law programming comprises the velocity estimation, the proper control law and other important elements needed for the practical implementation that will be developed from here.

The nominal case consists of the structure without changes (case 2). Two other cases are studied to evaluate the MR-STMD performance. Case 1 consists of adding four masses of 10 kg close to the mid-span, as shown in Figure 11a. Case 3 consists of reducing the span by moving the supports (reducing 20 cm at each side, a total reduction of 40 cm of the span) and removing the masses previously added (see Figure 11b). Table 5 shows the modal parameters of the beam for the three cases. Note that the MR-TMD and MR-STMD are tuned to case 2, and their ability to cancel vibration modes with lower and higher frequencies is studied.

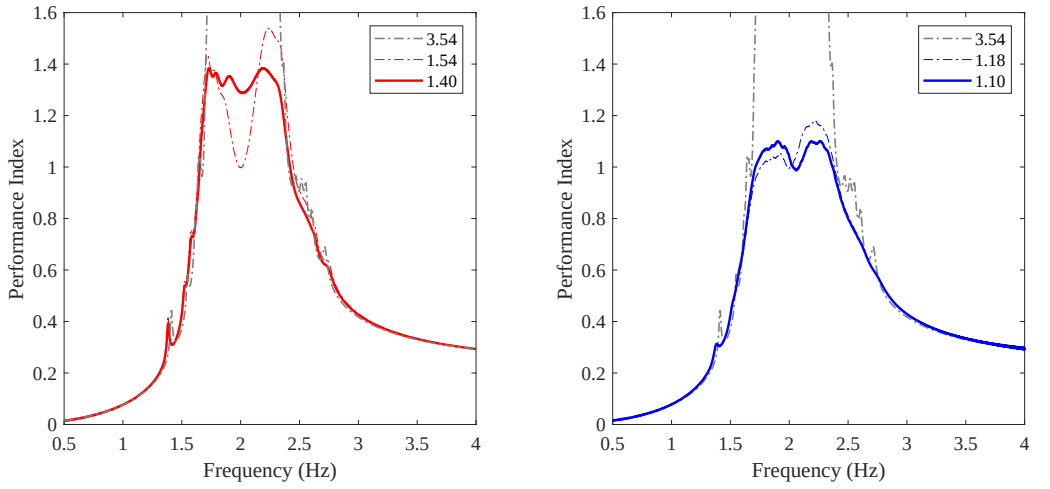

(a) MR-TMD. (b) MR-STMD.

FIGURE 10 Envelope curve and PI. Optimization for the case in which the Bingham MR damper model is included. The legend shows the PI values for these cases: (- - -) uncontrolled, (- - - -) initial solution and (——) optimized solution.

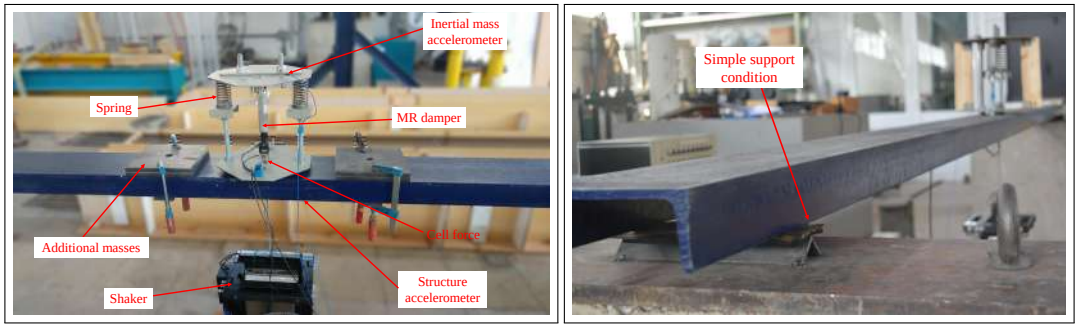

(a) General view. (b) Support view.

FIGURE 11 Description of the experimental test.

TABLE 5 Modal parameters of the beam for the three cases studied.

	Case 1	Case 2	Case 3
Frequency f_s (Hz)	5.67	6.65	7.67
Damping ratio ζ_s (%)	0.65	0.72	1.53
Modal mass m_s (kg)	115.15	76.87	63.80

4.2 | Mechanical design of Tuned Mass Damper

The Asami and Nishihara [30] solution serves as the initial estimate of the stiffness for the springs. Therefore, a physical model has been designed using two springs with a given stiffness of 2.5 kN/m each one and the MR damper identified in subsection 3.5. The inertial mass is set at 3 kg (mass ratio of 4% and tuned frequency of 6.49 Hz). A final tuning was carried out from the normalized spectrum using an excitation chirp from 3 and 8 Hz. This device is studied experimentally, functioning as passive control as well as semi-active control.

4.3 | Implementation of the control law

The practice implementation of the control law is described in this Section. Figure 12 shows the components of the inertial controller feedback (see Figure 2). The control force is $F_C = F_S + F_D$, F_S being the force of the springs and F_D the force of the damper. This control scheme has been implemented using a sampling frequency of 1000 Hz and assigned FIFO (First-In First-Out) conditions.

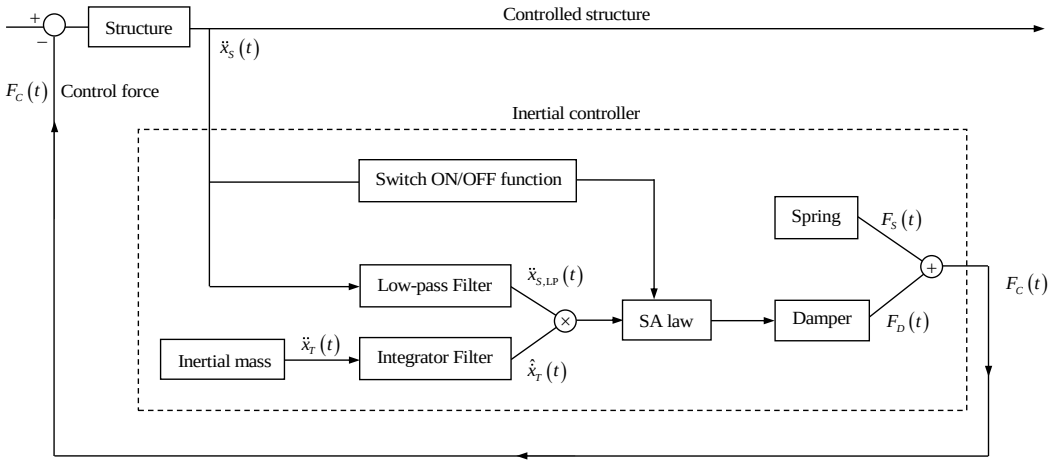

FIGURE 12 Control scheme for practical implementation of the inertial controller.

4.3.1 | Switching-on/off function

A switching-off function has been included to avoid continuous unnecessary operation of the control device. When the running RMS acceleration computed each second (see Eq. (12)) is under a certain value, the control law is OFF [35]. The switching-off function adopted here is $a_{\text{RMS},1} < 0.05\,\text{m/s}^2$.

4.3.2 | Low-pass filter

In order to avoid multiple unnecessary blocking/unblocking actions due to the noise of the acceleration of the structure at zero crossing, this signal is filtered by a low-pass Butterworth filter of 4^{th} order with a cut-off frequency of 100 Hz. This frequency should be high enough to prevent phase shifts in the structure acceleration that may spoil the

operation of the semi-active control law. Figure 13 shows the filtered acceleration for two cut-off frequencies of the low-pass filter. It is shown that the phase shift introduced by the 100 Hz cut-off frequency filter is negligible, whereas the high frequency noise is removed. Figure 14 shows the inertial mass acceleration together with the damper current as a result of applying the semi-active control law. In this figure, it can be seen that the blocking control action is applied uninterruptedly for a short time interval, that is, the damper brakes the inertial mass until tuning phase conditions are achieved.

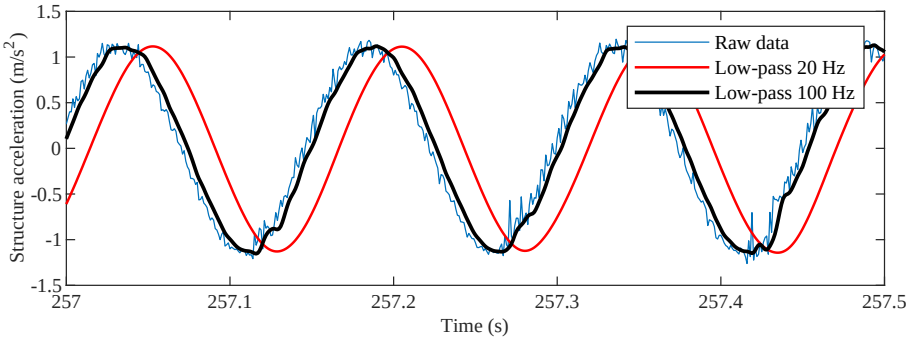

FIGURE 13 Original and low-filtered acceleration for two cut-off frequencies.

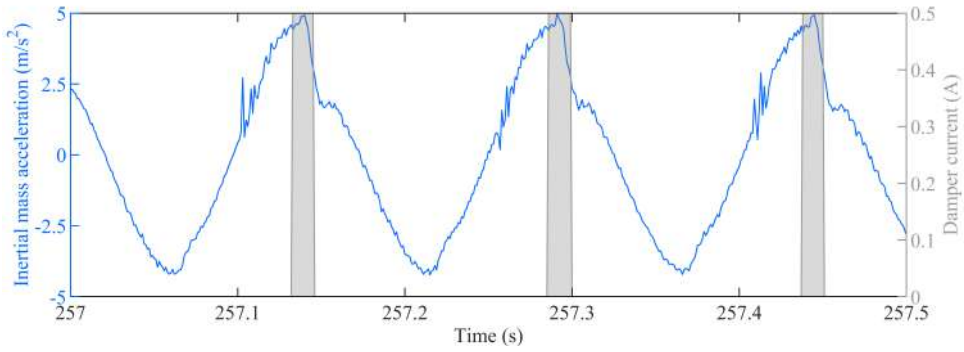

FIGURE 14 Braking the acceleration of the inertial mass due to the blocking force of the MR damper. The gray area represents the damper force turned on.

4.3.3 | Estimation of the inertial mass velocity

There are different ways to compute the estimated velocity of the inertial mass: i) a simple numerical differentiation of the displacement, ii) a Kinematic Kalman Filter (KKF) using the displacement and the acceleration [36, 37], and iii) a Leaky-Integrator Filter (LIF) using only the acceleration [38]. In the first case, differentiating a signal has the drawback that the noise levels can potentially be increased at the output, so this method is directly discarded. Also, it needs to measure the displacement while it is easier to measure accelerations. On the other hand, KKF is a more

robust method to estimate the velocity, but it has the disadvantage that both displacement and acceleration must be measured. Finally, an LIF is also a robust procedure for a harmonic signal (as usual for resonance response) and it only requires the acceleration to be measured. In addition, for the ON/OFF control law, only the velocity phase is actually important. The results of KKF and LIF have been experimentally compared, with similar results, making the LIF the most convenient method for the velocity estimation experimentally. Thus, the following integrator filter is adopted:

$$G(s) = \frac{s}{s^2 + 2\zeta_I \omega_I s + \omega_I^2}, \tag{16}$$

in which $s = j\omega$, ω being the angular frequency and ω_I and ζ_I are, respectively, the natural circular frequency and damping ratio of the integrator filter. The parameter ω_I should be chosen sufficiently smaller than ω_S to avoid significant phase shift at frequencies of interest. The parameters selected were $f_I = 0.5$ Hz and $\zeta_I = 1\%$. Then, $G(s)$ is transformed into the discrete domain using the zero-order hold with a sampling frequency of 1000 Hz, resulting in:

$$G(z) = \frac{0.0009969z - 0.0009969}{z^2 - 1.994z + 0.9937}, \tag{17}$$

where z is the discrete variable. Thus, this filter obtains the estimation of the velocity for frequencies greater than ω_I.

4.4 | Experimental tests

In this case, passive and semi-active vibration control is applied to the cases presented in subsection 4.1. The purpose of these tests is to prove the results obtained numerically for tuning the semi-active device. The damper current applied is 0.11 A for passive and 0.0 A for semi-active, since they have shown to be the optimal values for the nominal case.

Figure 15 shows the experimental results obtained for the three cases of Table 5. It shows the frequency domain response, magnitude (15a, 15b, and 15c) and phase (15d, 15e and 15f) between the structure acceleration and the excitation force for the structure without control and those controlled with the MR-TMD and with the MR-STMD. With respect to the magnitude, the MR-STMD shows a much better performance when out of the nominal case, although it also behaves better in the nominal case. It is really interesting to look at to the phase plots. The semi-active control law tries to correct the phase to keep the inertial mass velocity tuned to the structure acceleration (this results in a 90^o delay between the structure acceleration and the control force). Note that the phase correction in case 3 is less effective than in case 1. That is, when $\eta > 1$, the STMD frequency is higher than that of the structure and the semi-active control law is more effective, since it is easier to brake the inertial mass of the control device in this case (as opposed to $\eta < 1$). This result matches the results obtained in Table 2 and Table 4 from the optimization process for broad frequency-band vibration. It was demonstrated that the STMD frequency should be tuned at higher frequencies of the nominal structure frequency to cope with broad frequency-band vibrations.

Table 6 shows the reduction improvements obtained in the experimental tests. The improvement of the semi-active device with respect to the passive is also shown for each case. It can be seen that, although the semi-active device always improves the performance of the passive one, the greatest difference is obtained for case 1, in which the control device has a greater frequency than the structure. Finally, it should be mentioned that these results have come out as expected, according to the results obtained in the simulations carried out including the MR damper model.

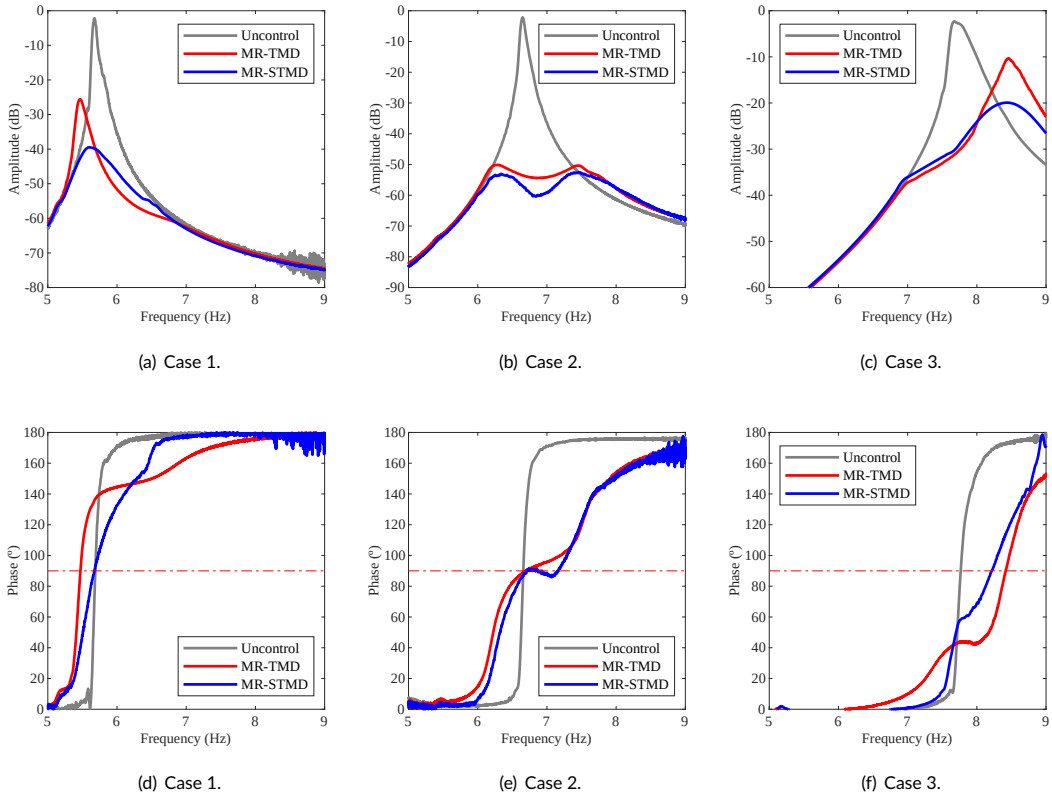

(a) Case 1. (b) Case 2. (c) Case 3.

(d) Case 1. (e) Case 2. (f) Case 3.

FIGURE 15 Experimental vibration results in frequency domain comparing the uncontrolled structure, MR-TMD and MR-TMD for the three cases of Table 5. The dashed red line (– – –) in the phase plots indicates 90^o delay between the structure acceleration and the control force, which means perfect tuning.

TABLE 6 Experimental vibration reduction (dB) for MR-TMD and MR-STMD for the three cases studied.

	Reduction (dB)		
Control device	**Case 1**	**Case 2**	**Case 3**
MR-TMD	23.94	49.01	8.20
MR-STMD	38.14	52.13	18.02
Improvement	**↑ 14.20**	**↑ 3.12**	**↑ 9.82**

5 | CONCLUSIONS

This paper presents a methodology for the tuning of STMDs to reduce vibrations in broadband-frequency-varying structures. The methodology is clearly geared to implementation since several practical issues are carefully considered. The methodology is convenient to both structures with an uncertain mode that may change over time or a structure

with several close-in-frequency modes.

The following conclusions can be drawn:

- For the sensitivity analysis:
  - The STMD is much less sensitive to structure parameter uncertainties than the TMD, thus showing a better performance for a given frequency band.
  - Regarding the damper force saturation, for the passive case, the force requirements are merely to dissipate the transferred energy, while the peak force needed is lower. In the semi-active case, higher requirements are needed.
- For the optimization analysis:
  - The STMD should be tuned at a higher frequency with a lower damping ratio than the TMD. That is, the TMD needs more damping to get a certain level of robustness. The higher frequency tuning of the STMD is due to the fact that it is easier for the semi-active controller to decelerate the inertial mass when its frequency is higher than the frequency of the structure.
  - If a model of an existing MR damper is included instead of a linear viscous damper, the performance is clearly degraded, although the STMD remains more robust and effective.
  - Table 7 shows a summary of all the results obtained for the different cases jointly: TMD, STMD, MR-TMD and MR-STMD. The aspects mentioned in the previous items are clearly appreciated in this Table.

TABLE 7 Summary of the results obtained numerically for TMD, STMD, MR-TMD and MR-STMD.

Control device	f_T (Hz)	PI	Reduction (%)
Uncontrolled structure	–	3.54	–
TMD	2.02	1.39	60.73
STMD	2.08	0.89	74.86
MR-TMD	2.02	1.40	60.45
MR-STMD	2.08	1.10	68.93

- For practical implementation:
  - To carry out practical implementations, three elements have been added to the semi-active control law: a switching-off function, a low-pass filter and an integrator filter. These elements increase the stability and reliability of the control system.
  - The effect of time delay for the MR damper to apply the semi-active control law can be considered negligible since the structure dynamics are much slower than the MR damper response, which always happen in lively low-frequency structures.
  - The experimental results support the previous numerical results. The phase control degrades faster for structures with a higher frequency than that of the STMD, which is why the tuned frequency of STMD should be higher than the nominal case.

Two future works are derived from this paper. The first is the implementation of this methodology on an in-service structure with several problematic modes in a frequency range. The second is to introduce the MR parameters into the optimization process. This will allow the best MR damper for a particular application to be found.

ACKNOWLEDGEMENTS

The authors acknowledge the financial support provided by the Ministry of Science, Innovation and Universities (Government of Spain) by funding the Research Project SEED-SD (RTI2018-099639-B-I00). The authors also acknowledge the partial financial support provided by the Research Net VIBRASTRUNET (BIA2015-71942-REDT). The authors acknowledge the computer resources and technical assistance provided by the "*Centro de Supercomputación y Visualización de Madrid*" (CeSViMa).

REFERENCES

[1] Den Hartog JP. Mechanical vibrations. Courier Corporation; 1985.

[2] Bachmann H, Weber B. Tuned Vibration Absorbers for Damping of Lively Structures. Structural Engineering International 1995;5(1):31–36.

[3] Ferreira F, Simões L. Least Cost Design of Curved Cable-Stayed Footbridges with Control Devices. Structures 2019;19(November 2018):68–83.

[4] SETRA/AFGC. Footbridges – Assessment of vibrational behaviour of footbridges under pedestrian loading. Technical Department for Transport, Roads and Bridges Engineering and Road Safety, Ministry of Transport and Infrastructure; 2016.

[5] Hu WH, Caetano E, Cuhna A. Structural health monitoring of a stress-ribbon footbridge. Engineering Structures 2012;47:578–593.

[6] Soria JM, Díaz IM, García-Palacios JH, Ibán N. Vibration Monitoring of a Steel-Plated Stress-Ribbon Footbridge: Uncertainties in the Modal Estimation. Journal of Bridge Engineering 2016;108(5):1175–1183.

[7] Hrovat D, Barak P, Rabins M. Semi-active versus passive or active tuned mass dampers for structural control. Journal of Engineering Mechanics 1983;109(3):691–705.

[8] Pinkaew T, Fujino Y. Effectiveness of semi-active tuned mass dampers under harmonic excitation. Engineering Structures 2001;23(7):850–856.

[9] Soria JM, Díaz IM, García-Palacios JH. Vibration control of a time-varying modal-parameter footbridge: study of semi-active implementable strategies. Smart Structures and Systems 2017;20(5):525–537.

[10] Koo JH, Shukla A, Ahmadian M. Dynamic performance analysis of non-linear tuned vibration absorbers. Communications in Nonlinear Science and Numerical Simulation 2008;13(9):1929–1937.

[11] Weber F, Maślanka M. Precise stiffness and damping emulation with MR dampers and its application to semi-active tuned mass dampers of Wolgograd Bridge. Smart Materials and Structures 2014;23(1).

[12] Ferreira F, Moutinho C, Cunha Á, Caetano E. Proposal of optimum tuning of semiactive TMDs used to reduce harmonic vibrations based on phase control strategy. Structural Control and Health Monitoring 2018;(November 2016):e2131.

[13] Caetano E, Cunha Á, Moutinho C, Magalhães F. Studies for controlling human-induced vibration of the Pedro e Inês footbridge, Portugal. Part 2: Implementation of tuned mass dampers. Engineering Structures 2010;32(4):1082–1091.

[14] Bortoluzzi D, Casciati S, Elia L, Faravelli L. Design of a TMD solution to mitigate wind-induced local vibrations in an existing timber footbridge. Smart Structures and Systems 2015;16(3):459–478.

[15] Nimmen KV, Verbeke P, Lombaert G, Roeck GD, Broeck PVD. Numerical and Experimental Evaluation of the Dynamic Performance of a Footbridge with Tuned Mass Dampers. Journal of Bridge Engineering 2016;21(8):1–14.

[16] Lievens K, Lombaert G, De Roeck G, Van den Broeck P. Robust design of a TMD for the vibration serviceability of a footbridge. Engineering Structures 2016;123:408–418.

[17] Jiménez-Alonso JF, Sáez A. Robust Optimum Design of Tuned Mass Dampers to Mitigate Pedestrian-Induced Vibrations Using Multi-Objective Genetic Algorithms. Structural Engineering International 2017;27(4):492–501.

[18] Mohebbi M, Shakeri K, Ghanbarpour Y, Majzoub H. Designing optimal multiple tuned mass dampers using genetic algorithms (GAs) for mitigating the seismic response of structures. Journal of Vibration and Control 2013;19(4):605–625.

[19] Weber F. Dynamic characteristics of controlled MR-STMDs of Wolgograd Bridge. Smart Materials and Structures 2013;22(095008):16pp.

[20] Ferreira F, Moutinho C, Cunha Á, Caetano E. Use of Semi-Active Tuned Mass Dampers to Control Footbridges Subjected to Synchronous Lateral Excitation. Journal of Sound and Vibration 2018;.

[21] Ferreira F, Simões L. Optimum Design of a Controlled Cable Stayed Footbridge Subject to a Running Event using Semi-active and Passive Mass Dampers. Journal of Performance of Constructed Facilities 2019;33(3):1–14.

[22] Weber F, Maślanka M. Frequency and damping adaptation of a TMD with controlled MR damper. Smart Materials and Structures 2012;21(5):055011.

[23] Dominguez A, Sedaghati R, Stiharu I. Modeling and application of MR dampers in semi-adaptive structures. Computers and Structures 2008;86(3-5):407–415.

[24] Soong TT, Dargush GF. Passive energy dissipation systems in structural engineering. Wiley New York; 1997.

[25] Koo JH, Ahmadian M, Setareh M, Murray T. In Search of Suitable Control Methods for Semi-Active Tuned Vibration Absorbers. Journal of Vibration and Control 2004;10(2):163–174.

[26] Chung L, Lai Y, Yang CW. Semi-active tuned mass dampers with phase control. Journal of Sound and Vibration 2013;332(15):1–16.

[27] Moutinho C. Testing a simple control law to reduce broadband frequency harmonic vibrations using semi-active tuned mass dampers. Smart Materials and Structures 2015;24(5):964–1726.

[28] Lai YA, Chung LL, Yang CSW, Wu LY. Semi-active phase control of tuned mass dampers for translational and torsional vibration mitigation of structures. Structural Control and Health Monitoring 2018;(November 2017):1–22.

[29] Moutinho C, Cunha Á, Caetano E, Martins De Carvalho J. Vibration control of a slender footbridge using passive and semiactive tuned mass dampers. Structural Control and Health Monitoring 2018;(November 2017):1–22.

[30] Asami T, Nishihara O. Closed-Form Exact Solution to H_∞ Optimization of Dynamic Vibration Absorbers (Application to Different Transfer Functions and Damping Systems). Journal of Vibration and Acoustics 2003;125(3):398.

[31] MATLAB. Version R2018b. Natick, Massachusetts: The MathWorks Inc.; 2018.

[32] Abramson MA. Pattern search algorithms for mixed variable general constrained optimization problems; 2002.

[33] ISO 2631–1. Mechanical Vibration and Shock: Evaluation of Human Exposure to Whole-body Vibration. Part 1, General Requirements, international standard ed.; 1997.

[34] Cesar MB, Barros RCD. Properties and Numerical Modeling of MR Dampers. In: 15th International Conference on Experimental Mechanics Porto, Portugal; 2012. .

[35] Díaz IM, Reynolds P. On-off nonlinear active control of floor vibrations. Mechanical Systems and Signal Processing 2010;24(6):1711–1726.

[36] Jeon S, Tomizuka M, Katou T. Kinematic Kalman filter (KKF) for robot end-effector sensing. Journal of dynamic systems, measurement, and control 2009;131(2):021010.

[37] Weber F, Bhowmik S, Høgsberg J. Extended neural network-based scheme for real-time force tracking with magnetorheological dampers. Structural Control and Health Monitoring 2014;(April 2013):225–247.

[38] Hudson MJ, Reynolds P. Implementation considerations for active vibration control in the design of floor structures. Engineering Structures 2012;44:334–358.